THE JOURNAL OF BIOLOGICAL CHEMISTRY VOL. 283, NO. 44, pp. 30401–30411, October 31, 2008

Structural Basis for a Distinct Catalytic Mechanism in *Trypanosoma brucei* Tryparedoxin Peroxidase*[S]

Received for publication, May 9, 2008, and in revised form, July 24, 2008 Published, JBC Papers in Press, August 6, 2008, DOI 10.1074/jbc.M803563200

Johannes Melchers[‡§], Michael Diechtierow[§], Krisztina Fehér[‡¶], Irmgard Sinning[§], Ivo Tews[§], R. Luise Krauth-Siegel[§], and Claudia Muhle-Goll[‡¶1]

From the [‡]Department of Structure and Biocomputing, EMBL, 69117 Heidelberg, Germany and the [§]Biochemie-Zentrum, Universität Heidelberg and the [¶]Max-Planck-Institut für Medizinische Forschung, 69120 Heidelberg, Germany

***Trypanosoma brucei*, the causative agent of African sleeping sickness, encodes three cysteine homologues (Px I–III) of classical selenocysteine-containing glutathione peroxidases. The enzymes obtain their reducing equivalents from the unique trypanothione (bis(glutathionyl)spermidine)/tryparedoxin system. During catalysis, these tryparedoxin peroxidases cycle between an oxidized form with an intramolecular disulfide bond between Cys[47] and Cys[95] and the reduced peroxidase with both residues in the thiol state. Here we report on the three-dimensional structures of oxidized *T. brucei* Px III at 1.4 Å resolution obtained by x-ray crystallography and of both the oxidized and the reduced protein determined by NMR spectroscopy. Px III is a monomeric protein unlike the homologous poplar thioredoxin peroxidase (TxP). The structures of oxidized and reduced Px III are essentially identical in contrast to what was recently found for TxP. In Px III, Cys[47], Gln[82], and Trp[137] do not form the catalytic triad observed in the selenoenzymes, and related proteins and the latter two residues are unaffected by the redox state of the protein. The mutational analysis of three conserved lysine residues in the vicinity of the catalytic cysteines revealed that exchange of Lys[107] against glutamate abrogates the reduction of hydrogen peroxide, whereas Lys[97] and Lys[99] play a crucial role in the interaction with tryparedoxin.**

Trypanosomes and *Leishmania*, the causative agents of several tropical diseases, have a unique thiol redox metabolism that is based on trypanothione (N^1,N^8-bis(glutathionyl)spermidine) and the flavoenzyme trypanothione reductase (for reviews, see Refs. 1 and 2). The parasites lack catalases and selenocysteine-containing glutathione peroxidases. 2-Cys-peroxiredoxins and cysteine-containing glutathione peroxidase-type enzymes are responsible for hydroperoxide reduction acting both as tryparedoxin peroxidases (for a recent review, see Ref. 3). With NADPH as primary electron source, the reducing equivalents flow via trypanothione and tryparedoxin (Tpx),[2] a distant relative of the thioredoxin protein family, onto the peroxidases which then reduce the hydroperoxide substrates (Scheme 1). In *Trypanosoma brucei*, the causative agent of African sleeping sickness, both the cytosolic 2-Cys peroxiredoxin and the glutathione peroxidase-type enzymes proved to be essential (4, 5).

Classical glutathione peroxidases (GPXs) are selenoproteins. Five distinct enzymes have been characterized in mammals, cytosolic GPX1, gastro-intestinal GPX2, plasma GPX3, phospholipid hydroperoxide peroxidase GPX4, and in humans, GPX6, which is restricted to the olfactory system (6). The high specificity of GPX1 for glutathione as reducing substrate gave the protein family its name (7). In the epididymis of rodents and monkeys, a GPX5 is expressed that contains an active site cysteine instead of the selenocysteine. Recently the structure of human GPX7, also a cysteine homologue, has been solved (PDB code 2P31). Expression of this gene is dramatically down-regulated in breast cancer cells (8). In general, cysteine-containing glutathione peroxidase-type enzymes are widespread in nature, and most of the enzymes, few of which are biochemically characterized, function as thioredoxin peroxidases (for reviews, see Refs. 9 and 10).

The selenoenzymes contain a catalytic triad. The selenoate of the peroxidatic selenocysteine is supposed to be stabilized by hydrogen bonds with a Gln and a Trp residue (11, 12). Site-directed mutagenesis (13) and computational studies (14, 15) supported the crucial role of the Gln and Trp residue for catalysis. Both residues are conserved over the entire family of glutathione peroxidase-type enzymes (Ref. 10; Fig. 1) with a few plant proteins having a Glu instead of Gln (16). This suggested that the cysteine-containing glutathione peroxidase-type enzymes are activated by a related mechanism (5, 16).

T. brucei encodes three nearly identical genes for cysteine-containing glutathione peroxidase-type tryparedoxin peroxidases (Px I-III) (17). The proteins occur in the cytosol and the

* This work was supported by Deutsche Forschungsgemeinschaft SFB 544, project B3 (to L. K.-S.). The costs of publication of this article were defrayed in part by the payment of page charges. This article must therefore be hereby marked "*advertisement*" in accordance with 18 U.S.C. Section 1734 solely to indicate this fact.

[S] The on-line version of this article (available at http://www.jbc.org) contains supplemental Figs. S1–S6.

The atomic coordinates and structure factors (codes 3dwv, 2rm5, and 2rm6) have been deposited in the Protein Data Bank, Research Collaboratory for Structural Bioinformatics, Rutgers University, New Brunswick, NJ (http://www.rcsb.org/).

[1] An Emmy Noether fellow of the Deutsche Forschungsgemeinschaft (Mu-1606-1). Present address and to whom correspondence should be addressed: Karlsruhe Institute of Technology, Institut für Biologische Grenzflächen (IBG-2), POB 3640, 76021 Karlsruhe, Germany. Tel.: 49-721-608-8700; Fax: 49-721-608-4823; E-mail: claudia.muhle@kit.edu.

[2] The abbreviations used are: Tpx, tryparedoxin; HSQC, heteronuclear single quantum correlation spectroscopy; GPX, classical selenocysteine-containing glutathione peroxidase; NOESY, nuclear Overhauser effect (NOE) spectroscopy; HetNOE, heteronuclear NOE; Px, glutathione peroxidase-type tryparedoxin peroxidase; r.m.s.d., root mean square deviation; TxP, glutathione peroxidase-type thioredoxin peroxidase.

mitochondrion of the parasites (5). In the mitochondrial Px III sequence, Cys^{47} replaces the selenocysteine residue. Substitution of Cys^{47} or Gln^{82} by a glycine residue resulted in inactive protein species, and the glycine mutant of Trp^{137} had only 12% wild type activity (18), which seemed to confirm the presence of the catalytic triad. Interestingly, in a related enzyme from Chinese cabbage, the respective glutamine to glycine mutation had no effect on peroxidase activity (19). Nearly all of the cysteine homologues, but not the selenoenzymes, possess a second cysteine (Cys^{95} in *T. brucei* Px III) that is essential for peroxidase activity (18, 19). In the first half reaction of catalysis, the thiolate form of Cys^{47} (reduced enzyme) reacts with the hydroperoxide substrate, resulting in the respective alcohol and probably a sulfenate at Cys^{47}. Attack of Cys^{95} generates an intramolecular disulfide bond (oxidized enzyme) that is in the second half reaction reduced by interaction with Tpx (Scheme 2).

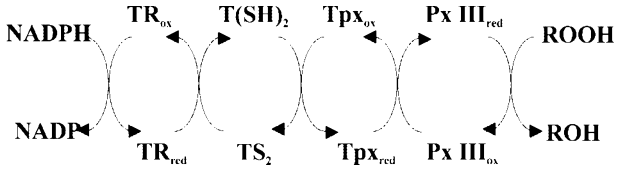

SCHEME 1. **In African trypanosomes, hydroperoxides (*ROOH*) are detoxified by a cascade composed of trypanothione reductase (*TR*), trypanothione ($T(SH)_2$), Tpx, and the Px III or a 2-Cys-peroxiredoxin.**

Here we present the crystal structure of oxidized *T. brucei* Px III and the NMR structures of the protein in oxidized and reduced form. Contrary to previous observations on poplar TxP (16), the closest homologue for which a three-dimensional structure has been published, *T. brucei* Px III does not undergo any significant structural rearrangement upon reduction of the intramolecular disulfide bridge. Furthermore, residues Gln^{82} and Trp^{137}, the residues equivalent to the catalytic triad in classical GPXs, are located far away from the active site Cys^{47} in our structures, ruling out the presence of the catalytic triad. Thus, the catalytic mechanism of Px III appears to differ fundamentally from any of the currently characterized enzymes. Analysis of the active site identified three lysines in the vicinity of the redox active cysteines that could play a role during catalysis. Kinetic analysis of three lysine mutants revealed that two of them, Lys^{97} and Lys^{99}, play a crucial role in the interaction with tryparedoxin, whereas Lys^{107} is involved in the first part of the reaction, the reduction of hydrogen peroxide.

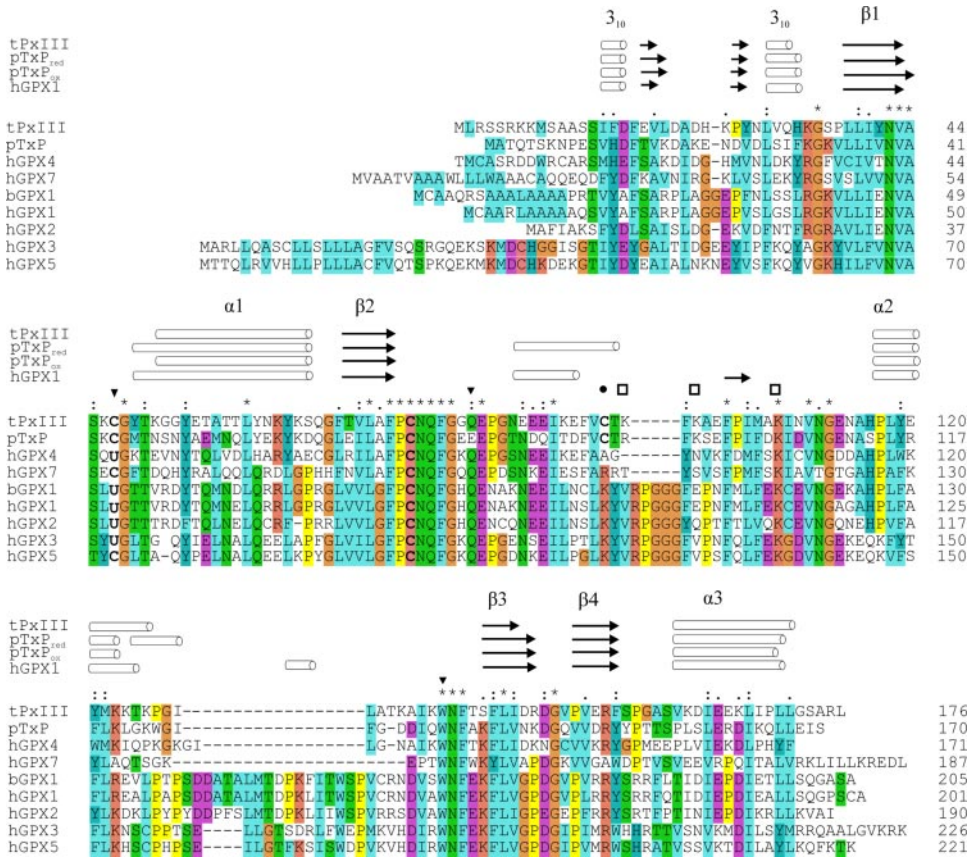

FIGURE 1. **Sequence alignment of *T. brucei* Px III with related peroxidases for which the three-dimensional structures are known.** The residues SeCys (*U*) or Cys, Gln, and Trp that form a catalytic triad in glutathione peroxidases and several cysteine-containing relatives are marked by *triangles*. Cysteine 95, which is essential for catalytic activity of Px III, is marked by a *filled circle*. The three Lys residues, Lys^{97}, Lys^{99}, and Lys^{107}, that were mutated in this work are marked by a *square*. α and 3_{10} helices (*rods*) as well as β-sheet regions (*arrows*) *above the alignment* refer to the secondary structures of Px III in comparison to reduced and oxidized poplar TxP ($pTxP_{red}$ and $pTxP_{ox}$) as well as human GPX1 (*hGPX1*). Residues that are identical in all sequences are marked by an *asterisk*, and highly or partially conserved residues by are marked by *colons* and *periods*, respectively. Cysteine residues are given in *bold letters*. The alignment was generated with ClustalX (57). *tPxIII*, *T. brucei* Px III (17); *pTxP*, *Populus trichocarpa* glutathione peroxidase 5 (PDB codes 2P5R and 2P5Q (16)); *hGPX4*, human GPX4 (2GS3 and 2OBI (42)); *hGPX7*, human GPX7 (2P31); *bGPX1*, bovine GPX1 (1GP1 (12)); *hGPX1*, human GPX1 (2F8A); hGPX2, human GPX2 (2HE3); *hGPX3*, human GPX3 (11); *hGPX5*, human GPX-5 (2IY3).

EXPERIMENTAL PROCEDURES

Materials—Recombinant *T. brucei* Tpx (20) and *Trypanosoma cruzi* trypanothione reductase (21) were prepared as described. Trypanothione disulfide was purchased from Bachem, and H_2O_2 was from Merck. $^{15}NH_4Cl$, [$^{13}C_6$]glucose and selectively labeled amino acids were obtained from Spectra Stable Isotopes.

Cloning, Expression, and Purification of Px III—For crystallization, the Ser^{76} mutant of Px III was expressed from the pQE30/*c76s-px III* plasmid which resulted in a protein species starting with Lys^{7}. The protein was prepared as described (17). For NMR studies, the Px III gene was cloned into a modified pET 9d vector with an N-terminal thioredoxin-His_6 tag cleavable by tobacco etch virus protease. The mitochondrial signal sequence of Px III was removed, and Cys^{76} was replaced by a serine residue which resulted in a fully active peroxidase (18) but excluded putative unspecific oxidation or dimerization. Details of the purification have been published elsewhere (22). The Ser^{47}, Ser^{95}, Glu^{97}, Gln^{97}, Glu^{99}, Gln^{99},

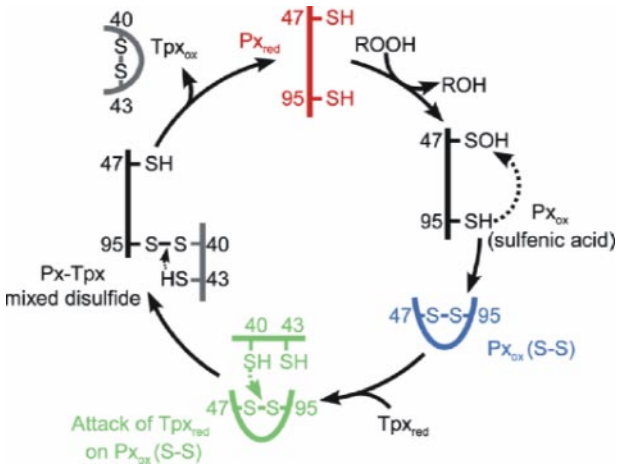

SCHEME 2. **Proposed reaction mechanism of Px III.** In the first half reaction, reduced Px III (Px_{red}) reacts with the hydroperoxide substrate (*ROOH*), and Cys^{47} becomes oxidized to a sulfenic acid (Px_{ox} (sulfenic acid)). Attack of Cys^{95} leads to formation of an intramolecular disulfide between Cys^{47} and Cys^{95} (Px_{ox} *(S-S)*). In the second half-reaction, Cys^{40} of reduced Tpx (Tpx_{red}) attacks Cys^{95} of the disulfide bond, resulting in an intermolecular disulfide between both proteins (*Px-Tpx mixed disulfide*). Cys^{43} of Tpx finally reacts with its vicinal Cys^{40} to release Px_{red} and oxidized Tpx (Tpx_{ox}). The three states of the catalytic cycle studied in this work, Px_{red}, Px_{ox} (S-S), and the complex between Tpx and PxIII are depicted in *red*, *blue*, and *green*, respectively.

and Glu^{107} mutants were generated using the QuikChange® mutagenesis kit (Stratagene) and the pET9d/*c76s-px III* or pET9d/*px III* plasmid as template. *Escherichia coli* XL1-Blue cells were transformed and grown at 37 °C in Luria-Bertani (LB) medium with 50 μg/ml kanamycin. The plasmid DNA was purified using the Nucleobond® PC100 kit (Macherey-Nagel). The recombinant Px III mutants were purified as described (22).

Structure Determination of the Oxidized State by X-ray Crystallography—Purified Px III was dialyzed against 100 mM Tris, 1 mM EDTA, pH 7.6, and concentrated to 13 mg/ml. The protein was crystallized by the hanging drop vapor diffusion method at 4 °C using a droplet size of 4 μl of Px III solution and 4 μl of the reservoir solution of 2 M ammonium sulfate, 0.1 M sodium acetate, pH 4.6. A crystal with an approximate size of $50 \times 50 \times 400$ μm^3 was shock-frozen under liquid nitrogen using mother liquor containing 20% glycerol as cryo protectant. Data were collected on beamline ID14-EH4 at the European Synchrotron Radiation Facility, Grenoble, France, at a wavelength of $\lambda = 0.9393$ Å (Table 1). A total of 500 frames with 0.25° oscillation were collected (*i.e.* 125° total). Toward higher resolution, diffraction spots were split, pointing to a potential twinning problem not readily detectable from the optical appearance of the crystals. Autoindexing, as implemented in denzo (23), suggested a centered orthorhombic cell with one molecule per asymmetric unit. Possible lower symmetries were centered monoclinic and primitive monoclinic with two or primitive triclinic with four molecules per asymmetric unit. Merging R-factors from scalepack (23) were 7.7% (C222), 6.1% (C2), 5.8% (P2), and 3.4% (P1). Data manipulation was carried out with the CCP4 package (24).

We used the ARP/wARP procedure of free atom density modification with subsequent auto-building (25) in the P2 lattice. Due to twinning, the model had to be completed in three steps by iterated model building in Coot (26) and ARP/wARP autotracing and refmac5 refinement (27). Twin refinement using the twin operator (-l, -k, -h) in shelxl (28) immediately reduced the R_{free} by more than 5% (Table 1); the twin fraction refined to 0.473. Model correction and introduction of anisotropic refinement reduced the R_{free} by a further 3%. Model building and refinement were carried out similarly to the serine protease example given in the shelx manual. The initial 491 water molecules, assigned by the ARP/wARP procedure, were reduced in the course of refinement to 365 water molecules to avoid fitting of noise; in refinement cycles 3 and 5, the automated water-divining procedure of shelx was used with default/recommended settings.

NMR Experiments—The chemical shift assignment has been published elsewhere (22). For structure determination, two-dimensional NOESY in 100% D_2O, ^{15}N HSQC-NOESY, and ^{13}C heteronuclear multiple quantum coherence-NOESY spectra were recorded at high field (800/900 MHz) with mixing times of 80 ms (oxidized form) and 100 ms (reduced form) at 22 °C and a protein concentration of 1 mM. Data were processed with NMRPIPE (29) and analyzed using NMRVIEW (30). Structures were calculated with ARIA1.2/CNS (31) on the basis of the experimentally derived NOE restraints (Table 2). Additional dihedral restraints derived from TALOS analysis (32) of the chemical shifts and hydrogen bonds identified on the basis of characteristic NOE patterns (Table 2) were added. The water-refined structures were examined with PROCHECK (33). Figures were prepared with MOLMOL (34) and PyMOL (35).

To analyze the two conformations of the reduced enzyme, 300 μM Px III in 50 mM sodium phosphate, 100 mM KCl, pH 6.8, was treated with 10 mM dithiothreitol, and the NMR-tube was purged with argon to prevent reoxidation. Constant reducing conditions were verified by subjecting an aliquot of the solution to thiol determination with 5,5-dithiobis(2-nitrobenzoate). The difference in chemical shift $\Delta\delta$ was calculated with the formula $\Delta\delta = \sqrt{(\delta H^2 + (\delta N/10)^2)}$. One-dimensional ^1H NMR spectra were recorded at 600 MHZ between 29 and 4 °C in D_2O and H_2O. To evaluate if the appearance of two conformations was pH-dependent, the Px III solution was titrated to pH 5.0, 6.8, and 9.5 with 1 M HCl or NaOH. The role of Cys^{47} and Cys^{95} was studied by alkylating the protein at pH 8.0 with 15 mM iodoacetamide in the presence of 2 mM dithiothreitol.

Kinetic Analysis of the Px III Lysine Mutants—Peroxidase activity was measured at 25 °C in a total volume of 150 μl of 0.1 M Tris, 5 mM EDTA, pH 7.6, in the presence of 240 μM NADPH, 100 μM trypanothione disulfide, 150 milliunits of trypanothione reductase, 10 μM Tpx, and 0.1–0.9 μM concentrations of the different Px III species. The reaction was started by adding 100 μM H_2O_2, and NADPH consumption was followed at 340 nm (5, 17). The kinetic parameters were determined by Dalziel kinetics as described for the wild type enzyme (17). The Tpx concentration was varied between 2 and 10 μM in the presence of 0.2 and 0.6 μM Px III. The reactions were started by the addition of 60 μM H_2O_2.

Modeling of the Complex between Px III and Tpx—The 10 lowest energy NMR structures of oxidized Px III and the x-ray structure of oxidized *Trypanosoma brucei* Tpx (PDB code

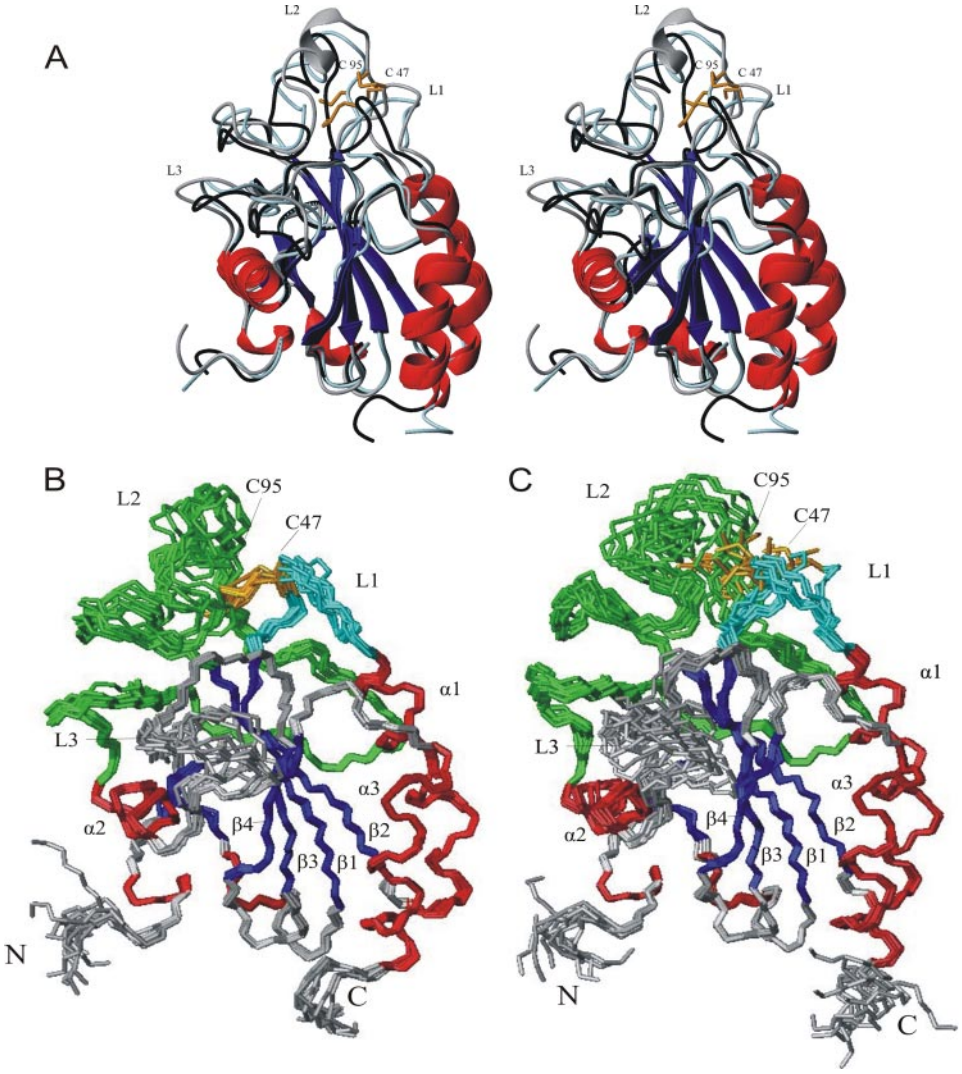

FIGURE 2. **Structures of oxidized and reduced Px III.** *A*, stereo image of the superposition of the structures of oxidized Px III obtained by x-ray and NMR analysis (*gray* and *black*, respectively) and the NMR-structure of reduced Px III (*light blue*). α-Helices and 3_{10}-helices are colored in *red*, and β-sheets are in *blue*. The two catalytically active cysteine residues Cys^{47} and Cys^{95} are depicted in *orange*. The α-helix in loop 2 only present in the crystal structure is shown in *gray*. *B* and *C*, ensemble of the 10 lowest energy NMR structures of 200 calculated structures after water refinement for the oxidized and reduced protein, respectively. The three most extended loops are given in *cyan* (*L1*, loop 1; Ala^{44}–Lys^{51}), *green* (L2, loop 2; Ser^{76}-His^{116}) and *gray* (L3, loop 3; Lys^{126}-Thr^{140}). *N* and *C* mark the N and the C terminus of the protein.

1O73 (36)) were used to model the complex structure. The docking was performed using HADDOCK 2.0 (37, 38). The solvated docking was carried out with the recommended parameters of HADDOCK. Cys^{40} of Tpx and Cys^{95} of Px III were defined as active residues. During the rotational and translational rigid body minimization docking, 1000 structures were calculated with solvation. The best 200 solutions according to intermolecular energy were used for the semi-flexible annealing in torsion angle space. This was followed by a final refinement with explicit modeling of hydrating water molecules. The resulting 200 structures were clustered on the basis of the intermolecular van der Waals, electrostatic, and restraint energy terms, buried surface area, desolvation energy, and binding energy as combined in the HADDOCK score *versus* the backbone r.m.s.d. from the lowest HADDOCK score structure. The HADDOCK score is a weighted sum of various energy terms obtained in different phases of the docking. The energy terms include van der Waals energy, electrostatic energy, ambiguous distance restraints energy, buried surface area, binding energy and desolvation energy. The structure with the smallest weighted sum, that is, with the smallest HADDOCK score, is ranked first. Solvent surface accessibility was determined by NACCES 2.1.1 (39). Intermolecular interactions were analyzed with LIGPLOT (40).

RESULTS

Overall Structure of T. brucei Px III—We determined the structure of oxidized *T. brucei* Px III both by x-ray crystallography at a resolution of 1.4 Å and by NMR spectroscopy (Fig. 2). For the structural analyses, Cys^{76} of Px III was replaced by a serine residue which resulted in a fully active enzyme species (18). The structure of the reduced form was obtained only by NMR spectroscopy. The statistics of the structure determinations by x-ray and NMR are presented in Tables 1 and 2, respectively.

The x-ray and NMR structures of oxidized Px III (Fig. 2*A*) are highly similar, with a r.m.s.d. over the backbone atoms of 0.63 Å. The crystal structure revealed a dimer in the asymmetric unit. The buried surface has been determined with CNS (41) to be 1160 $Å^2$. The interface comprises the loops from Gly^{81} to Glu^{88} and from Gly^{128} to Trp^{137} as well as Asn^{111}. Trp^{137} is involved in hydrophobic interactions in the dimer; in classical GPXs, this residue is in hydrogen-bonding distance to the catalytic selenocysteine instead. The localization of Trp^{137} at the dimer interface leads to two different conformations for the indole ring, neither of which corresponds to the conformation observed by NMR. To assay whether the dimer occurs at higher concentrations or is driven by crystal packing, ^1H T2 spin-echo relaxation measurements and pulsed-field-gradient NMR diffusion measurements were performed. They yielded a relaxation time and diffusion coefficient typical for a monomeric protein at 1 mM concentration (14.1 ± 1.5 ms at 21 °C, $D_s = 0.953 \pm 0.008 \times 10^{-6}$ cm^2s^{-1}, supplemental Figs. 1 and 2, respectively) corroborating previous gel chromatography results in which Px III eluted as a monomer (17).

Minor differences between the x-ray and the NMR structure were observed for loop 1 (Ala^{44}–Lys^{51}) and loop 3 (Lys^{126}–

Thr[140], Fig. 2*A*). Well defined NOE contacts from Ser[45] to Pro[75] and Ser[76] lead to an altered orientation of loop 1 in the NMR structure. Because loop 1 and loop 2 (Ser[76]–His[116]) are connected via the intramolecular disulfide between Cys[47] and Cys[95], loop 2 and the entire catalytic region are shifted as a consequence (Fig. 2*A*). Loop 3 is involved in the hydrogen bonding contacts between monomers in the crystal, which leads to a different conformation.

TABLE 1

Data collection and refinement statistics of the X-ray structure of oxidized Px III

HR, high resolution bin; $R_{sym} = \Sigma_h\Sigma_i|I(h) - I(h)_i|/\Sigma_h\Sigma_i I(h)_i$, where $I(h)$ is the mean intensity after rejections; $R_{work} = \Sigma_h||F_{obs}(h)| - |F_{calc}(h)||/\Sigma h|F_{obs}(h)|$, where $F_{obs}(h)$ and $F_{calc}(h)$ are the observed and calculated structure factors, respectively. 5% of the data were excluded to calculate R_{free}.

Data collection statistics	
Space group	$P2_1$
Unit cell *a*, *b*, *c* (Å), b (°)	42.8 × 105.9 × 42.8, 100.5
Resolution (Å)/HR bin (Å)	50-1.41/1.43-1.41
R_{sym} (%)/HR (%)	5.8/47.3
$I/\sigma(I)$/HR	14.9/2.1
Completeness (%)/HR (%)	99.2/96.8
Redundancy/HR	2.6/2.5
Unique reflections	71,308
Average B (Å^2)	14.6
Refinement statistics	
R_{work} (%)/R_{free} (%)	12.6/19.4
Residues in model	A and B, Met-9–Leu-171
No of amino acids with double conformations	32
No of protein atoms/waters	2,782/358
r.m.s.d. bond length (Å)/angle (°)	0.011/0.030
Ramachandran statistics	
Most favored (residues/%)	89.2
Additional favored (residues/%)	10.4
Generously allowed (residues/%)	0.4
Disallowed (residues/%)	0.0

In the x-ray structure, Glu[88]–Glu[92] form an α-helical turn (Fig. 2*A*), which coincides with α-helix 2 in GPXs (Fig. 1) and reduced poplar TxP (16). Because NMR data reflect the average of all possible conformations, it is conceivable that this part of loop 2 has some potential of α-helix formation.

The monomeric state of Px III is in agreement with the fact that it lacks a long stretch (inserted between Ile[129] and Leu[130]) that forms the subunit interface in the tetrameric GPXs (Refs. 11 and 12; Fig. 1). This loop is not present in the monomeric human GPX4 (PDB code 2GS3 and 2OBI (42)) as well as in most of the cysteine-containing glutathione peroxidase-type proteins including poplar TxP (16). Nevertheless, the latter forms a homodimer (42, 43). This protein dimerizes through the C-terminal region (16). Most of the residues localized in the interface are conserved in related plant proteins but not in Px III.

Px III displays a high loop content of about 60% (Figs. 1 and 2). The overall fold of Px III is 3_{10}-β-β-3_{10}-β^1-α-β^2-α-β^3-β^4-α instead of the common 3_{10}-β-β-3_{10}-β^1-α-β^2-α-β-α-β^3-β^4-α-fold of other GPX-type proteins, because it lacks an α-helix and a short β-sheet found in distinct GPX structures between β-sheet 2 and α-helix 2. This region with the redox active Cys[95] forms a loop of more than 30 residues (loop 2; Cys[76]–Leu[118]).

Active Site Structure of Px III—Cys[47] and Cys[95] form the redox active dithiol/disulfide couple, which in the oxidized enzyme forms an intramolecular disulfide (Ref. 18; Figs. 2*A* and 3*A*). In both oxidized and reduced Px III, the peroxidatic Cys[47] is located on the first loop (L1) between β-strand 1 and α-helix 1, whereas the resolving Cys[95] is part of the long loop 2 (L2) between β-sheet 2 and α-helix 2 that is relatively disordered in the bundle of NMR structures (Figs. 2, *B* and *C*). Both residues

TABLE 2

Structural statistics of the NMR structures of oxidized and reduced Px III

	$\langle SA_{ox}\rangle^a$	$\langle SA_{ox}^{watref}\rangle^b$	$\langle SA_{red}\rangle^a$	$\langle SA_{red}^{watref}\rangle^a$
Distance restraints				
All NOEs (unambiguous/ambiguous)	4273/51		4627/46	
Intraresidual	1328		1315	
Sequential ($\|i - j\| = 1$)	791		868	
Medium range ($1\langle\|i - j\| \leq 4$)	619		792	
Long range ($\|i - j\|\rangle 4$)	1596		1702	
Dihedral angles $\phi\psi$	89/89		89/89	
H bonds	44		44	
r.m.s.d. (Å) from experimental restraints[c]				
All distance restraints	0.07 ± 0.01	0.06 ± 0.01	0.04 ± 0.01	0.04 ± 0.01
Dihedral angles[d]	2.63 ± 0.21	2.63 ± 0.28	2.78 ± 0.29	2.50 ± 0.26
Coordinate precision (Å)[e]				
N, C^α, C′	1.02 ± 0.20	0.84 ± 0.20	1.36 ± 0.36	1.03 ± 0.12
All heavy atoms	1.59 ± 1.24	1.38 ± 0.22	2.02 ± 0.30	1.63 ± 0.23
Structural quality[f], bad contacts	14.75 ± 2.38	3.05 ± 0.76	12.00 ± 2.83	3.20 ± 0.70
Ramachandran plot				
Residues in most favored region (%)	69.3 ± 2.0	77.0 ± 2.0	68.1 ± 2.0	72.4 ± 2.3
Residues in additionally Allowed region (%)	24.1 ± 2.5	17.4 ± 2.2	24.0 ± 2.1	21.6 ± 2.5
Residues in generously allowed region (%)	4.3 ± 1.6	3.9 ± 1.2	5.0 ± 2.1	3.3 ± 1.5
Residues in disallowed Region (%)	2.3 ± 1.2	1.7 ± 1.0	2.9 ± 1.9	2.7 ± 1.3

[a] $\langle SA_{ox}\rangle$ and $\langle SA_{red}\rangle$ are ensembles of the 20 lowest energy solution structures (out of 200 calculated) of Px III in the oxidized and reduced state before water refinement, respectively.

[b] $\langle SA_{ox}^{watref}\rangle$ and $\langle SA_{red}^{watref}\rangle$ are the $\langle SA\rangle$ ensembles after refinement in a shell of water (31). The CNS E_{repel} function was used to simulate van der Waals interactions with an energy constant of 25 kcal mol^{-1} Å^{-4} using PROLSQ van der Waals radii; r.m.s.d. for bond length, bond angles, and improper dihedral angels are 0.0034 (±0.0001) Å, 0.581 (±0.015)°, and 0.578 (±0.021)° before and 0.0052 (±0.0002) Å, 0.697 (±0.020)°, and 2.24 (±0.11)° after water refinement (oxidized form) and 0.0047 (±0.0001) Å, 0.657 (±0.011)°, and 0.634 (±0.017)° before and 0.0063 (±0.0002) Å, 0.761 (±0.016)°, and 2.27 (±0.10)° after water refinement (reduced form).

[c] Distance restraints were employed with a soft square-well potential using an energy constant of 50 kcal mol^{-1} Å^{-2}. No distance restraint in the $\langle SA_{ox}\rangle$ and $\langle SA_{red}\rangle$ was violated by more than 0.2 Å.

[d] Dihedral angle restraints derived from TALOS (32) were applied to ϕ,ψ backbone angles using energy constants of 200 kcal mol^{-1} rad^{-2}.

[e] Coordinate precision is given as the Cartesian coordinate r.m.s.d. of the 20 lowest energy structures in the NMR ensemble with respect to their mean structure for residues 15–179 of Px III.

[f] Structural quality was analyzed using PROCHEK.

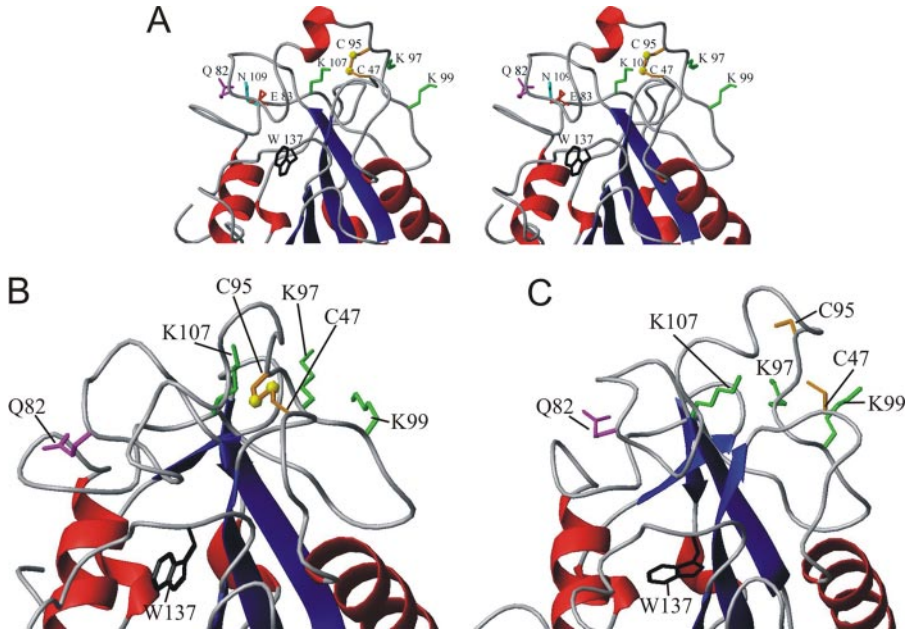

FIGURE 3. **Details of the catalytic site.** *A*, stereo image of the x-ray structure of oxidized Px III showing the details of the active site. Trp^{137} (*black*) does not interact with Cys^{47}. Lys^{97}, Lys^{99}, and Lys^{107} that were mutated in this work are depicted in *green*. Gln^{82} (*magenta*) on loop 2 is 16.7 Å apart from the disulfide bridge and is, thus, unable to interact with the cysteines. Instead, its side chain amide is in hydrogen bond distance to the carboxylate group of Glu^{83} (*red*), which in turn is 2.9 Å distance from the side chain amide of Asn^{109} (*cyan*). Thus, Gln^{82} is part of a network of hydrogen bonds and thereby may stabilize the orientation of Cys^{95}. *B* and *C*, details of the redox active part in a representative NMR structure of the oxidized (*B*) and reduced (*C*) Px III, respectively.

are surface-exposed and are, thus, freely accessible to large hydroperoxide substrates as well as to tryparedoxin. Px III contains three solvent-exposed aromatic residues (Tyr^{49}, Phe^{79}, and Phe^{93}). Two of them (Tyr^{49} and Phe^{93}) are located close to the redox active cysteines. Because aromatic residues usually pack into the core of a protein, this may indicate that these residues are involved in the binding of protein partners. An aromatic residue at position 93 is found in most of the monomeric members of the protein family (Ref. 10, Fig. 1), whereas Tyr^{49} is not conserved. Interestingly, Cys^{47} and Cys^{95} of Px III are located in the center of a negatively and positively charged surface patch formed by Glu^{87}, Glu^{88}, Glu^{89}, Glu^{92} and Lys^{46}, Lys^{97}, Lys^{99}, Lys^{107}, respectively. The residues of these charged patches are partially conserved (Fig. 1).

In the selenocysteine-containing peroxidases, the active site selenoate is in hydrogen bonding distance to the indole $N_\epsilon H$ of the tryptophan and the $N_\epsilon H$ amide group of the glutamine of the catalytic triad. The corresponding residues are conserved throughout the entire protein family (Fig. 1) (11–13, 42). However, in all of our three structures of Px III, Trp^{137} and Gln^{82} are not found in the immediate vicinity of the cysteines (the distance between the C_α atom of Cys^{47} and the side chain nitrogen atoms of Trp^{137} or Gln^{82} are 16 and 16.7 Å; Fig. 3, *A*–*C*). According to the NMR data, Trp^{137} is surface-exposed, with only a few NOEs to Leu^{130}, Lys^{136}, and Ser^{155}. In the x-ray structure, the side chain amide of Gln^{82} is in hydrogen-bonding distance to the carboxylate group of Glu^{83}, which forms a hydrogen bond with the side chain amide of Asn^{109} (Fig. 3*A*), concomitantly stabilizing loop 2 that harbors Cys^{95}. In the NMR structures of both the oxidized and reduced protein, the side chain orientation of Gln^{82} could not be determined to high precision due to spectral overlap of its resonances, but the rough orientation of Gln^{82} defined by a few isolated NOEs in both structures superimposed well with the crystallographic data (Fig. 3, *A*–*C*). Thus, despite the conservation of Gln^{82} and Trp^{137} and the fact that the Gly^{82} and Gly^{137} mutants of *T. brucei* Px III had 2 and 12% wild type activity, respectively (18), in Px III the two residues are too far away from the redox active cysteine residues to contribute to a stabilization of the thiolate anion of Cys^{47}.

Structure of Reduced Px III—Superposition of the $^1H,^{15}N$ HSQC fingerprint spectra of the reduced and oxidized protein revealed that numerous residues underwent significant chemical shift changes, and several resonances disappeared due to exchange broadening (Fig. 4*A*). Most of these are located close to the redox active cysteines (Fig. 4*B*). To identify which peaks disappeared due to exchange broadening and which ones shifted into highly overlapping regions, selectively labeled samples of $[^{15}N]$Ala/$[^{15}N]$Lys, $[^{15}N]$Thr, $[^{15}N]$Phe, $[^{15}N]$Tyr, and $[^{13}C,^{15}N]$Cys were prepared and analyzed. For the selectively labeled $[^{13}C,^{15}N]$Cys protein, two resonances were detected as expected in the oxidized protein. Upon reduction, both signals disappeared completely. Removal of dithiothreitol restored the cysteine signals (supplemental Fig. S3).

Overall, the structures of the oxidized and reduced protein superimposed well (Fig. 2*A*). The r.m.s.d. over the backbone atoms between reduced and oxidized structures was 0.59 Å. Thus, most of the secondary chemical shifts do not originate from structural changes, *e.g.* the signals of Ile^{40} and Tyr^{41} (Fig. 4*A*) shift although they are located in the core of the protein. Large secondary chemical shifts can be attributed to the flanking regions of the two cysteines (Fig. 4*B*). Inspection of the structure revealed that they are essentially caused by the formation of the disulfide bridge and probably a slight rotation of the neighboring aromatic side chains of Phe^{93} and Phe^{98}. Substantial structural rearrangements were not observed for the catalytic region in accordance with comparable NOE patterns in the oxidized and reduced protein for residues of loop 1 and 2. The residues between Gln^{82} and Lys^{97} do not have long range NOEs either in oxidized or in reduced Px III, and their ^{13}C Cα- and Cβ chemical shifts were comparable in both redox states. This rules out that loop 2, rather separated from the core of the protein in our structures, rearranges into an α-helix in reduced Px III, as found for poplar TxP (16).

Trp^{137} and Gln^{82} are likewise unaffected by the redox state of the protein as both the NOE pattern and especially the more sensitive chemical shifts did not differ between oxidized and

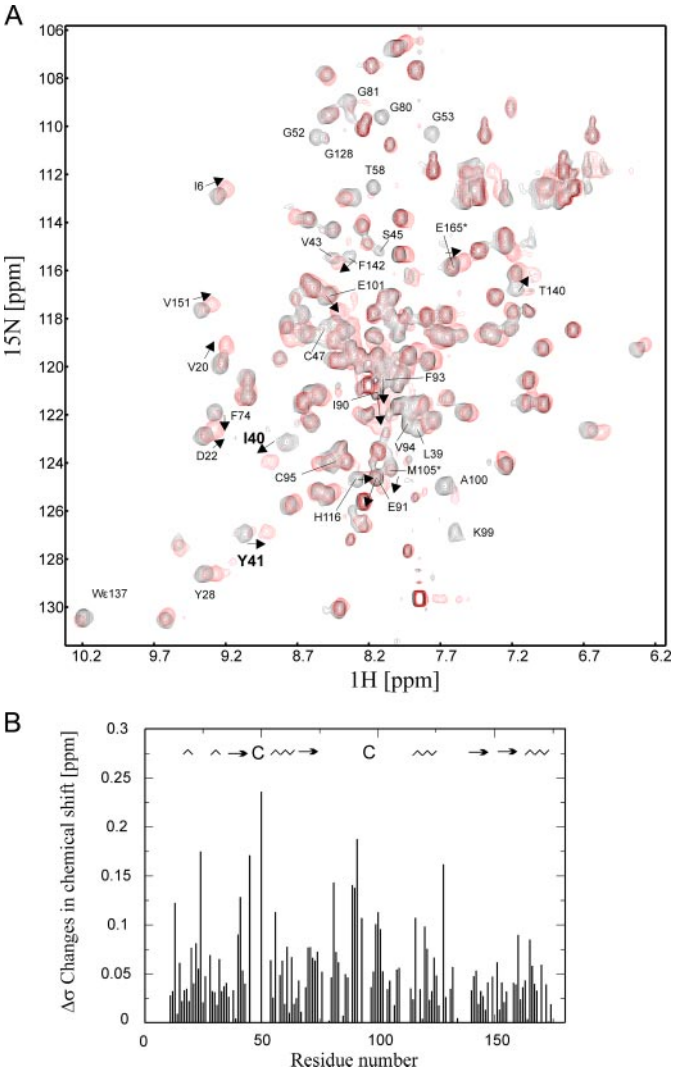

FIGURE 4. **Comparison of the $^{1}H^{15}N$ HSQC spectra of oxidized and reduced Px III.** *A*, superposition of the $^{1}H^{15}N$ HSQC spectra of oxidized (*black*) and reduced (*red*) Px III. Several residues (marked by *arrows*) are shifted upon reduction or experience line-broadening. *B*, chemical shift difference between oxidized and reduced Px III plotted onto the sequence. The secondary structure of Px III is shown at the *top* of the figure (∧, α- and 3_{10}-helices; →, β-sheets).

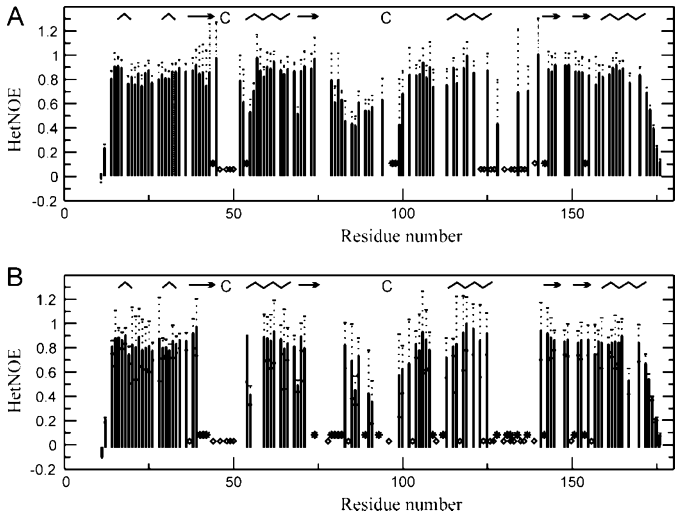

FIGURE 5. **The three loops are mobile in both oxidized and reduced Px III.** HetNOE analysis of oxidized (*A*) and reduced (*B*) Px III are shown. Residues where line-broadening affected accurate determination of the HetNOE value are marked by *stars*. Residues that were exchange-broadened beyond detection are depicted as *diamonds*. Empty fields denote that the residues cannot be analyzed due to spectral overlap. The secondary structure of Px III is shown at the top of the figure (∧, α- and 3_{10}-helices; →, β-sheets).

reduced protein. In the reduced protein signals obtained for Trp^{137} were exchange broadened (but still detectable), indicating higher flexibility. The tryptophan fluorescence emission spectra of reduced and oxidized Px III were identical (supplemental Fig. S4), corroborating that the protein environment around the single tryptophan residue does not change significantly. The spectra of the Ser^{47} and Ser^{95} mutants showed the same emission maximum, further highlighting that the environment of Trp^{137} is unaffected by formation of the intramolecular disulfide bridge. The fluorescence emission maximum at 344 nm is in accordance with a rather solvent-exposed position of Trp^{137}. In the presence of 6 M guanidinium hydrochloride, the emission maximum of the reduced protein was 360 nm (not shown). Thus, denaturing only slightly further increases the hydrophilicity around Trp^{137}.

The Three Loops and the Adjacent Regions Are Flexible—In the oxidized Px III, the H_N/N resonances of several residues in the vicinity of the catalytic cysteines or Trp^{137} were line-broadened, some of them (Lys^{46}, Gly^{48} to Lys^{51}, Asn^{77}, Gln^{78}, Thr^{96}, Ile^{110}, Gly^{112}, Leu^{130}, Lys^{133}, Lys^{136} to Phe^{139}) beyond detection. In the reduced state, these regions extend to further residues covering the entire loop 1 and parts of loop 2 and loop 3 (Ala^{44}–Cys^{47}, Gly^{52}, Gly^{53}, Ala^{57}, Gly^{81}, Val^{94}, Cys^{95}, Phe^{98}, and Gly^{128} are additionally broadened) (Fig. 4*A*). To rule out that an overlap of the signals in crowded regions of the spectrum prevented their detection, Px III was labeled with either [^{15}N]Ala/[^{15}N]Lys, [^{15}N]Thr, [^{15}N]Phe, [^{15}N]Tyr, or [^{13}C,^{15}N]Cys. In the spectra of the selectively labeled samples simplified that way (^{1}H,^{15}N HSQC, ^{15}N-edited NOESY), the H_N/N resonances were indeed missing, proving that they are exchange-broadened. Such a phenomenon is often caused by motion in the micro- or millisecond range. To compare the motion in both oxidized and reduced protein, we studied the backbone dynamics. The ^{1}H,^{15}N HetNOE values (Fig. 5) of the residues at the edges of the exchange-broadened loops 2 and 3, which contain Cys^{95} and Trp^{137}, respectively, displayed lower values (down to 0.4) compared with the overall HetNOE of 0.8- 0.9 in both oxidized and reduced protein. Unfortunately, line-broadening effects and also spectral overlap prevented analysis of the motion in more detail.

Thus, the reason that the loops 2 and 3 are not well defined in both NMR structures is not only due to the fact that the respective residues have a low number of long range NOEs but reflects true mobility. It is not surprising that opening of the disulfide bridge leads to an increase in the mobility of the loops. This could also account for the overall low stability of the reduced protein. However, a significant motion is already present in the oxidized form and appears to be an intrinsic feature of the enzyme.

Evidence for Two Conformations in the Reduced Protein—When analyzing the two-dimensional NOESY spectra of reduced Px III acquired at high field (900 MHz, 22 °C), we

TABLE 3

Kinetic constants for the reduction of hydrogen peroxide by wild type and mutant Px III species

The Dalziel coefficient Φ_0 (the *ordinate* intercept in the secondary plot, see supplemental Fig. S6*C*) equals E_o/V_{max} that is $1/k_{cat}$. Φ_1 (the slope of the primary plot, supplemental Fig. S6, *A* and *B*) corresponds to $1/k_1'$, and Φ_2 (the slope of the secondary plot, supplemental Fig. S6*C*) corresponds to $1/k_2'$. The k_1' and k_2' values refer to the overall rate constants for the oxidation and reduction of the peroxidase, respectively. K_m1 (Φ_1/Φ_0) and K_m2 (Φ_2/Φ_0) represent the K_m values for hydrogen peroxide and tryparedoxin, respectively. The values are the mean of three independent series of experiments. ND, not determined.

Px III	Activity	Φ_0	Φ_1	Φ_2	k_{cat}	k_1'	k_2'	K_m1	K_m2
	%	*s*	$\mu M\ s$	$\mu M\ s$	s^{-1}	$\mu M^{-1}s^{-1} \times 10^4$	$\mu M^{-1}s^{-1} \times 10^5$	μM	μM
Wild type	100	0.63	10.3 ± 2.4	2.0	1.7	9.7 ± 3.0	5.1	18 ± 4	3.4
Glu^{97}	12	1.93	15.9 ± 7.0	20.5	0.5	6.3 ± 5.0	0.5	8 ± 4	10.7
Glu^{99}	36	1.41	17.4 ± 7.0	10.6	0.7	6.3 ± 6.0	0.9	12 ± 7	7.5
Glu^{107}	2	15.5	3000 ± 320	2.3	0.1	0.0003	4.4	1930 ± 20	0.1
Gln^{97}	58	ND	ND	ND	ND	ND	ND	ND	ND
Gln^{99}	59	ND	ND	ND	ND	ND	ND	ND	ND

observed a duplication of at least 20 resonances that showed an exactly identical twin NOE pattern originating from two conformations. The intensities of the two conformations were comparable. Residues affected by the duplication extended well into the core of the protein. One-dimensional spectra acquired at different pH values or after carboxyamidomethylation of the cysteines revealed that the duplication arose from the redox active cysteine (supplemental Fig. S5). The analysis of the Ser^{47} and Ser^{95} mutants confirmed this. The ratio of the two conformations varied with temperature (studied range 4–29 °C), pH, and H_2O *versus* D_2O, *e.g.* at 4 °C, one conformation was dominant, whereas at 29 °C both populations were of similar intensity. Thus, instead of two irreversibly modified distinct species, we observed two interchanging conformations. Although the phenomenon awaits further accurate exploration, our data suggest that the two conformations observed in the reduced protein are caused by protonation/deprotonation of the cysteines, which might be relevant for the catalytic mechanism of the enzyme.

Conserved Lysine Residues Specifically Affect Catalysis—In the three structures of Px III, Lys^{97}, Lys^{99} (both conserved in trypanosomatid and related plant proteins), and Lys^{107} (conserved throughout the entire protein family) are located in the vicinity of the redox active dithiol/disulfide on the surface of the protein pointing outward with their N_zH_3 groups (Figs. 3, *A–C*). To elucidate if these residues play a role in catalysis, Lys^{97} and Lys^{99} were replaced by glutamine and all three lysine residues by glutamate. One-dimensional spectra confirmed that the mutations did not affect the overall protein structure.

Gln^{99}, Glu^{99}, and Gln^{97} Px III showed 40–60% and Glu^{97} Px III 12% remaining activity, whereas Glu^{107} Px III had only 2% wild type activity left (Table 3). The expression system introduced in this work yielded Px III species that were significantly more stable than the previously prepared recombinant protein (5, 17, 18). In addition, the wild type enzyme obtained here exerted a three times higher specific activity and displayed saturation kinetics. To investigate which of the two half reactions, namely the reduction of H_2O_2 by reduced Px III or the regeneration of reduced Px III by Tpx (Scheme 2), is affected by the replacement of the lysines, wild type, Glu^{97}, Glu^{99}, and Glu^{107} Px III were subjected to a detailed kinetic analysis (as shown for Glu^{97} and wild type Px III in supplemental Fig. S6). The K_m values and the apparent second order rate constant k_1' of wild type, Glu^{97}, and Glu^{99} Px III were in the same order of magnitude, whereas the k_2' value of Glu^{97} and Glu^{99} Px III was 10 and 5 times lower than that of the wild type enzyme, respectively (Table 3). This suggests that Lys^{97} and Lys^{99} play a role in the interaction between oxidized Px III and reduced Tpx.

Strikingly, replacement of Lys^{107} did not influence the interaction with Tpx (k_2') but caused a drop of the k_1'-value by more than 3 orders of magnitude and, thus, severely affected the reduction of H_2O_2. Because Glu^{107} Px III slowly reduced H_2O_2, the disulfide bond between Cys^{47} and Cys^{95} can still be formed. Otherwise Cys^{47} should have been irreversibly over-oxidized. As shown previously, reaction of Ser^{95} Px III with a stoichiometric concentration of H_2O_2 generates a sulfinic acid at Cys^{47} (18). Probably the nucleophilic attack of Cys^{47} on the peroxide substrate is impaired.

Because our structures do not reveal direct contact between Cys^{47} and Lys^{107}, structural changes in loop 1 or loop 2 may account for the observed changes. In 14 of the 20 lowest energy NMR structures of reduced Px III, Lys^{107} interacts with the backbone or side chain hydroxyl group of Ser^{45} and/or Thr^{96} and, thus, stabilizes the conformation of these loops. Ser^{45} in its turn could activate Cys^{47} by another hydrogen bond. However, since the side chain resonances of Lys^{107} are found in highly overlapping areas of the NOESY spectra, this hypothesis needs a final confirmation by mutational analysis.

Modeling of the Interactions between Px III and Tpx—The structure of the complex between Px III and Tpx was modeled using HADDOCK (37, 38). The starting structures were the lowest energy NMR structure of the oxidized Px III and the x-ray structure of oxidized *T. brucei* Tpx (PDB code 1O73 (36)). In the absence of a structure of reduced Tpx, this approach seems justified because reduction of Tpx from *C. fasciculata* has only minor effects (36, 44). The expected structural change between oxidized and reduced Tpx was taken into account by defining the active site WCPPC motif fully flexible during the second stage of the docking.

Mass spectrometry data revealed that the intermolecular disulfide bridge is formed between Cys^{95} of Px III and Cys^{40} of Tpx (18). The two cysteines were, hence, treated as the center of the interaction. To create a tightly connected complex structure, the thiol hydrogen atoms of the reactive cysteines were removed, leaving more space for the sulfur atoms to approach each other. Lys^{97} and Lys^{99} of Px III were also incorporated in the interaction surface because of the mutagenesis results (Table 3).

The complex structure (Fig. 6*A*) contains 4 salt bridges, 1 hydrogen bond, and 21 hydrophobic contacts as identified by LIGPLOT (40). The buried surface area at the contact between the two protein molecules is 1350.46 $Å^2$. The HADDOCK score

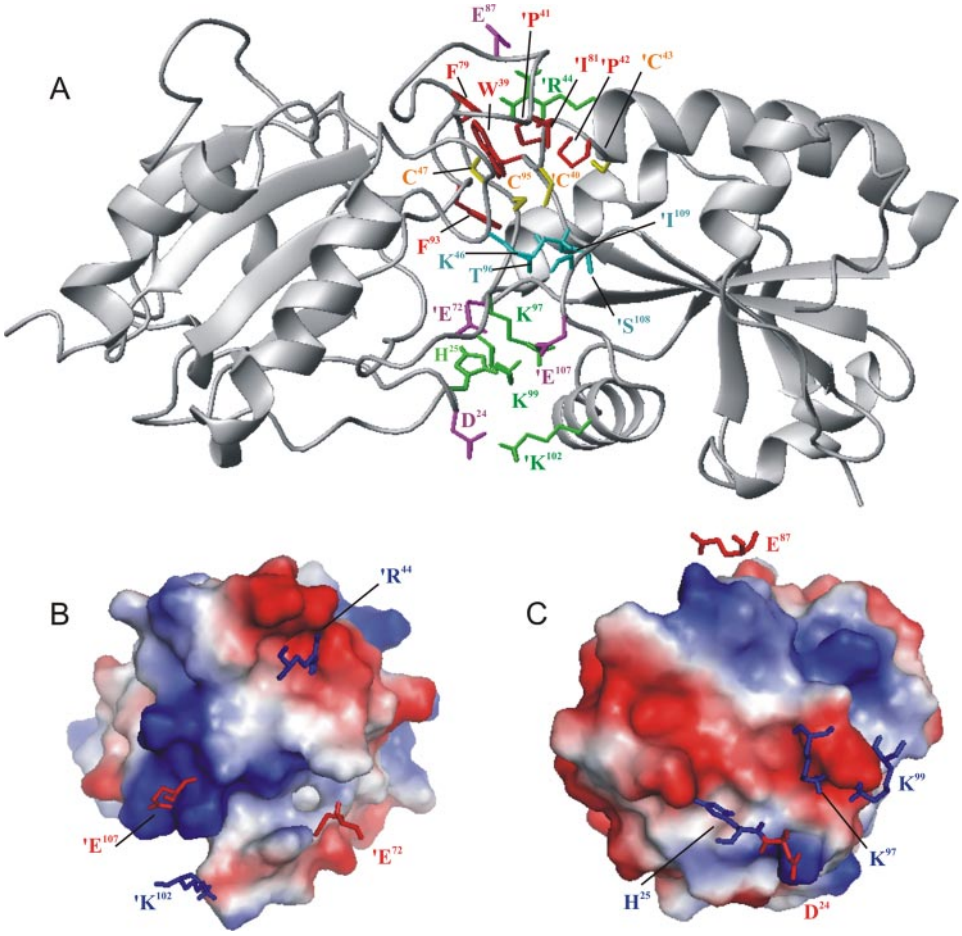

FIGURE 6. **Model of the complex between Px III and Tpx.** The complex between Px III (*left*) and Tpx (*right*, *primed residues*) as derived from the docking calculation (*A*) is shown. Potential intermolecular contacts are shown. *Yellow*, cysteines; *green*, positively (*green*); *magenta*, negatively charged residues involved in salt bridges (Lys^{97} and Lys^{99} of Px III with Glu^{107} of Tpx, Asp^{24} of Px III with Lys^{102} of Tpx, Glu^{83}, Glu^{87}, and Glu^{88} of Px III with Arg^{44} of Tpx); *cyan*, residues involved in hydrogen bonds (Thr^{96} of Px III with the backbone of Ile^{109} of Tpx); *red*, residues undergoing hydrophobic contacts (Phe^{79}, Val^{94}, and Phe^{93} of Px III with Trp^{39}, Pro^{41}, and Pro^{42} of Tpx). *B* and *C*, electrostatic surface of the proteins calculated with PyMOL (35) showing the electrostatic interactions between charged residues at the interface. *B*, the side chains of Tpx that interact with Px III are displayed together with a surface representation of Px III. *C*, same for side chains of Px III that interact with Tpx.

achieved was ~140 units as calculated from the weighted average of different parameters as described under "Experimental Procedures." Vacuum electrostatic charges on the contacting surface are shown in Figs. 6, *B* and *C*. The cross-sections of the molecules revealed complementary electrostatic charges at the binding interface. Lys^{97} and Lys^{99} of Px III, identified by our mutational screen to interact with Tpx, are involved in a salt bridge with Glu^{107} of Tpx. This could explain why the Gln mutants retained a higher activity than the respective Glu mutants. Glutamine residues could still interact with the glutamate of Tpx through formation of hydrogen bonds, whereas the proximity of glutamate residues should lead to electrostatic repulsion.

DISCUSSION

Eight structures of glutathione peroxidase-type enzymes are currently available. The majority of them (bovine GPX1 and human GPX1–4) represent the classical selenoenzymes, either the authentic proteins or mutants where the selenocysteine is replaced by different residues. The other two structures show cysteine-containing homologues (human GPX5 and GPX7), but these proteins lack a second redox active cysteine and, thus, are unable to form an intramolecular disulfide bridge. Thioredoxin-dependent poplar TxP is the only peroxidase that, as does Px III, cycles between a reduced dithiol form and an oxidized form containing an intramolecular disulfide bridge (16).

Poplar TxP undergoes a remarkable structural rearrangement upon oxidation previously observed for both typical and atypical 2-Cys peroxiredoxins (Refs. 45 and 46, and for a comprehensive review, see Ref. 47). The reduced form shows a catalytic triad with Glu^{82} and Trp^{133} stabilizing the peroxidatic cysteine analogous to GPXs (16). Upon oxidation, α-helix 3 unwinds, which leads to a long loop that extends from the core of the protein and allows the peroxidatic cysteine to approach the resolving one to form a disulfide bridge, disrupting the arrangement of the catalytic triad. Although the monomeric *T. brucei* Px III and the dimeric poplar TxP show 48% overall sequence identity, our structural data revealed that Px III does not undergo such a dramatic conformational change. Reduced and oxidized Px III have essentially the same structure, and the conserved Gln^{82} and Trp^{133} do not form a catalytic triad with Cys^{47}. This was demonstrated by the unchanged chemical shifts for both residues and identical NOE patterns, especially for Trp^{137}, loop 1, and loop 2.

Treatment of reduced Px III with 0.5 mM glutathione disulfide leads to glutathionylation of either Cys^{47} or Cys^{95} but not of both residues in the same protein molecule (48). Modification of one cysteine probably interferes sterically with the modification of the second one in accordance with the structural data that also in the reduced form of Px III both cysteines lie in close proximity. This would allow the rapid condensation between the sulfenic acid formed at Cys^{47} upon hydroperoxide reduction and the thiol of Cys^{95} generating the intramolecular disulfide bond of the oxidized enzyme.

The different catalytic mechanism of *T. brucei* Px III and the poplar TxP is further corroborated by the tryptophan fluorescence of the proteins. Whereas the spectra of poplar TxP reflect a switch from a hydrophobic environment in the reduced state to an exposed conformation in the oxidized state (43), the tryptophan fluorescence emission spectra of oxidized and reduced Px III are identical and in accordance

with an exposed position of Trp^{137} in both forms (supplemental Fig. S4).

Is it possible that despite a sequence identity of nearly 50%, the structures differ so considerably? The paradigm of homology modeling efforts and structural genomic initiatives is that related sequences lead to homologous structures (49) hoping that prediction can mostly replace tedious structure determination. In general, a sequence identity of 50% is regarded as a good basis for a relatively safe prediction. However, a recent publication indicates that this goal is not always achievable. Bryan and co-workers inter-converted all residues of a G_A and a G_B domain of protein G, a cell wall protein from *Streptococcus.* 5 of 45 residues were shown to be sufficient to change the structure of an 3-α-helix-fold into an α/β-fold (50). Likewise, the insertion of three further residues into the sequence converts Gal3p, a protein of the GAL pathway in *Saccharomyces cerevisiae*, from a transcriptional inhibitor to an activator of the pathway, changing it into a galactokinase (51). Thus, small changes in the protein sequence can lead to huge and crucial differences in the three-dimensional structure or function that render predictions not entirely reliable.

The NMR structure of oxidized and reduced Px III revealed that the three loops containing Cys^{47}, Cys^{95}, and Trp^{137} are highly flexible, especially in the reduced protein. In particular, the residues between Gln^{82} and Phe^{98} do not show long range NOEs, in accordance with loop 2 not being intimately connected to the core of the protein. Previous studies of Akke and Kern and co-workers (52) have revealed that enzymes may not have to rearrange their enzymatic pockets in an induced fit but that the substrate appears to select the correct one among many allowed conformations. A similar mechanism could be the case for Px III. Binding of a substrate could trap one conformation leading to a stabilization of the loops. Unfortunately, hydroperoxides are rather unstable, so that this could not be investigated by NMR or x-ray analyses. The fact that several residues show line-broadening in the $^{1}H^{15}N$ HSQC spectra corroborates the idea that these loops and adjacent regions undergo micro- or millisecond motions. Upon formation of the disulfide bridge, the entire structure is stabilized, which is reflected in the higher thermal stability and the overall higher quality of the NMR spectra. When the disulfide bridge opens, the loops may undergo a swaying motion.

In the structures of Px III, Cys^{47}, Gln^{82}, and Trp^{137} are located far apart from each other and not in direct contact, excluding the formation of the canonical catalytic triad. The specific role of these residues is also not easy to analyze in other members of the family because they are not necessarily conserved, at least in the cysteine-containing glutathione peroxidase-type enzymes. In TxP, the glutamine residue of the catalytic triad is replaced by a glutamate (Glu^{79}), but the structural arrangement is comparable with that in the selenocysteine enzymes. A respective mutation in GPX4 severely affected the catalytic efficiency of the protein (13, 42), but in the TxP of Chinese cabbage (19), a glutamine to glycine mutation resulted in a fully active enzyme species.

One interesting aspect is how the peroxidatic Cys^{47} is activated. In many cases the low pK value of a specific cysteine residue is difficult to explain. Despite a number of known structures and detailed biochemical studies, it is still not clear why the N-terminal Cys of the C*XX*C motif in glutaredoxins has a p*K* value significantly lower than that of a free cysteine, whereas the p*K* value of the C-terminal active site Cys has a p*K* value higher than that of free cysteine (53). A common hypothesis is that conserved basic residues (Arg^{26} and Lys^{19} in pig glutaredoxin) (54) or an arginine in peroxiredoxins (55) stabilize the thiolate of the more N-terminal cysteine (54). However, a recent molecular dynamics simulation suggests that cationic side chains contribute little to the activation. Instead, the thiolate appears to be stabilized by the backbone NH groups of the two following residues (53). The structures of Px III did not reveal any positively charged residue in the vicinity of the active site thiolate, and one may speculate that the thiolate of Cys^{47} in reduced Px III is also stabilized by interaction with the backbone. However, one should bear in mind that due to a lack of unambiguous NOEs of the residues close to Cys^{47}, the exact orientation of several residues in the active site could not be determined by NMR.

The active site of Px III shows a very open conformation. The immediate environment of the redox active dithiol/disulfide is formed exclusively by residues of the loops 1 and 2 that contain Cys^{47} and Cys^{95}, respectively. In comparison, the active sites of poplar TxP as well as of GPX1, GPX3, and GPX4 also comprise residues of the loops between α-helix 2 and β-strand 3 as well as between β-strand 4 and α-helix 3 in Px III (11, 16). Furthermore, the active site of these enzymes is shielded by an adjacent subunit. The exposed redox active cysteines of Px III would render the protein perfectly suited for interactions with bulky substrates and may also be a prerequisite for an efficient reduction by Tpx.

Glutathione peroxidase-type peroxidase-3 in yeast does not act only as a hydroperoxide scavenger but also as a hydroperoxide sensor (56). The sulfenic acid residue generated in the peroxidase reacts with a cysteine of the transcription factor Yap1. This intermolecular disulfide is then transposed to an intramolecular disulfide in Yap1, causing its activation. Future work will reveal if Px III is part of a redox signaling cascade in trypanosomes.

The PDB coordinates have been deposited under accession numbers 3dwv (oxidized protein, x-ray structure), 2rm5 (oxidized protein, NMR structure), 2rm6 (reduced protein, NMR structure).

Acknowledgments—The modified pET-vector was kindly provided by Gunter Stier, EMBL. We thank Dr. Tanja Schlecker for helping with the crystallization of the peroxidase. We further thank staff at the European Synchrotron Radiation Facility, Grenoble, France, Dr. Klemens Wild, BZH Heidelberg for help with X-ray data collection, and Dr. Thomas Barends, MPI for Medical Research, Heidelberg, for helpful discussions on crystal twinning. High field NOESY spectra were recorded at the Frankfurt Facility for Biomolecular NMR, which is funded by the European Union project "EU-NMR-European Network of Research Infrastructures for Providing Access and Technological Advancement in Bio-NMR" (FP-2005-RII3 Contract 026145).

Note Added in Proof—While this manuscript was under revision, Fairlamb and colleagues published the crystal structure of reduced *T. brucei* Px II (2VUP; Alphey, M. S., König, J., and Fairlamb, A. H. (2008) *Biochem. J.* 414, 375–381). This structure is similar to the crystal structure of the poplar TxP but differs from our solution structure in the details of the catalytic site. Future work is needed to resolve the discrepancies between the structures.

REFERENCES

1. Fairlamb, A. H., and Cerami, A. (1992) *Annu. Rev. Microbiol.* **46,** 695–729
2. Krauth-Siegel, R. L., Bauer, H., and Schirmer, R. H. (2005) *Angew. Chem. Int. Ed. Engl.* **44,** 690–715
3. Krauth-Siegel, R. L., Comini, M. A., and Schlecker, T. (2007) *Subcell. Biochem.* **44,** 231–251
4. Wilkinson, S. R., Horn, D., Prathalingam, S. R., and Kelly, J. M. (2003) *J. Biol. Chem.* **278,** 31640–31646
5. Schlecker, T., Schmidt, A., Dirdjaja, N., Voncken, F., Clayton, C., and Krauth-Siegel, R. L. (2005) *J. Biol. Chem.* **280,** 14385–14394
6. Brigelius-Flohé, R. (2006) *Biol. Chem.* **387,** 1329–1335
7. Brigelius-Flohé, R., and Flohé, L. (2003) *Biofactors* **17,** 93–102
8. Utomo, A., Jiang, X., Furuta, S., Yun, J., Levin, D. S., Wang, Y. C., Desai, K. V., Green, J. E., Chen, P. L., and Lee, W. H. (2004) *J. Biol. Chem.* **15,** 43522–43529
9. Herbette, S., Roeckel-Drevet, P., and Drevet, J. R. (2007) *FEBS J.* **274,** 2163–2180
10. Maiorino, M., Ursini, F., Bosello, V., Toppo, S., Tosatto, S. C., Mauri, P., Becker, K., Roveri, A., Bulato, C., Benazzi, L., De Palma, A., and Flohé, L. (2007) *J. Mol. Biol.* **365,** 1033–1046
11. Ren, B., Huang, W., Akesson, B., and Ladenstein, R. (1997) *J. Mol. Biol.* **268,** 869–885
12. Epp, O., Ladenstein, R., and Wendel, A. (1983) *Eur. J. Biochem.* **133,** 51–69
13. Maiorino, M., Aumann, K. D., Brigelius-Flohé, R., Doria, D., van den Heuvel, J., McCarthy, J., Roveri, A., Ursini, F., and Flohé, L. (1995) *Biol. Chem.* **376,** 651–660
14. Aumann, K. D., Bedorf, N., Brigelius-Flohé, R., Schomburg, D., and Flohé, L. (1997) *Biomed. Environ. Mass Spectrom.* **10,** 136–155
15. Prabhakar, R., Vreven, T., Morokuma, K., and Musaev, D. G. (2005) *Biochemistry* **44,** 11864–11871
16. Koh, C. S., Didierjean, C., Navrot, N., Panjikar, S., Mulliert, G., Rouhier, N., Jacquot, J. P., Aubry, A., Shawkataly, O., and Corbier, C. (2007) *J. Mol. Biol.* **370,** 512–529
17. Hillebrand, H., Schmidt, A., and Krauth-Siegel, R. L. (2003) *J. Biol. Chem.* **278,** 6809–6815
18. Schlecker, T., Comini, M. A., Melchers, J., Ruppert, T., and Krauth-Siegel, R. L. (2007) *Biochem. J.* **405,** 445–454
19. Jung, B. G., Lee, K. O., Lee, S. S., Chi, Y. H., Jang, H. H., Kang, S. S., Lee, K., Lim, D., Yoon, S. C., Yun, D. J., Inoue, Y., Cho, M. J., and Lee, S. Y. (2002) *J. Biol. Chem.* **277,** 12572–12578
20. Lüdemann, H., Dormeyer, M., Sticherling, C., Stallmann, D., Follmann, H., and Krauth-Siegel, R. L. (1998) *FEBS Lett.* **431,** 381–385
21. Sullivan, F. X., and Walsh, C. T. (1991) *Mol. Biochem. Parasitol.* **44,** 145–147
22. Melchers, J., Krauth-Siegel, R. L., and Muhle-Goll, C. (2008) *Biomol. NMR Assignments* **2,** 65–68
23. Otwinowski, Z., and Minor, W. (1997) *Methods Enzymol.* **276,** 307–326
24. Collaborative Computational Project (1994) *Acta Crystallogr.* **50,** 760–763
25. Perrakis, A., Morris, R., and Lamzin, V. S. (1999) *Nat. Struct. Biol.* **6,** 458–463
26. Emsley, P., and Cowtan, K. (2004) *Acta Crystallogr.* **60,** 2126–2132
27. Murshudov, G. N., Vagin, A. A., and Dodson, E. J. (1997) *Acta Crystallogr.* **53,** 240–255
28. Sheldrick, G. M. (2008) *Acta Crystallogr.* **64,** 112–122
29. Delaglio, F., Grzesiek, S., Vuister, G. W., Zhu, G., Pfeifer, J., and Bax, A. (1995) *J. Biomol. NMR* **6,** 277–293
30. Johnson, B. A., and Blevins, R. A. (1994) *J. Biomol. NMR* **4,** 603–614
31. Linge, J. P., O'Donoghue, S. I., and Nilges, M. (2001) *Methods Enzymol.* **339,** 71–90
32. Cornilescu, G., Delaglio, F., and Bax, A. (1999) *J. Biomol. NMR* **13,** 289–302
33. Laskowski, R. A., Rullmannn, J. A., MacArthur, M. W., Kaptein, R., and Thornton, J. M. (1996) *J. Biomol. NMR* **8,** 477–486
34. Koradi, R., Billeter, M., and Wüthrich, K. (1996) *J. Mol. Graph.* **14,** 29–32
35. DeLano, W. L. (2002) *DeLano Scientific*, Palo Alto, CA
36. Alphey, M. S., Gabrielsen, M., Micossi, E., Leonard, G. A., McSweeney, S. M., Ravelli, R. B., Tetaud, E., Fairlamb, A. H., Bond, C. S., and Hunter, W. N. (2003) *J. Biol. Chem.* **278,** 25919–25925
37. Dominguez, C., Boelens, R., and Bonvin, A. M. (2003) *J. Am. Chem. Soc.* **125,** 1731–1737
38. de Vries, S. J., van Dijk, A. D., Krzeminski, M., van Dijk, M., Thureau, A., Hsu, V., Wassenaar, T., and Bonvin, A. M. (2007) *Proteins* **69,** 726–733
39. Hubbard, S. J., Campbell, S. F., and Thornton, J. M. (1991) *J. Mol. Biol.* **220,** 507–530
40. Wallace, A. C., Laskowski, R. A., and Thornton, J. M. (1995) *Prot. Eng.* **8,** 127–134
41. Brünger, A. T., Adams, P. D., Clore, G. M., DeLano, W. L., Gros, P., Grosse-Kunstleve, R. W., Jiang, J. S., Kuszewski, J., Nilges, M., Pannu, N. S., Read, R. J., Rice, L. M., Simonson, T., and Warren, G. L. (1998) *Acta Crystallogr. D. Biol. Crystallogr.* **54,** 905–921
42. Scheerer, P., Borchert, A., Krauss, N., Wessner, H., Gerth, C., Höhne, W., and Kuhn, H. (2007) *Biochemistry* **46,** 9041–9049
43. Navrot, N., Collin, V., Gualberto, J., Gelhaye, E., Hirasawa, M., Rey, P., Knaff, D. B., Issakidis, E., Jacquot, J. P., and Rouhier, N. (2006) *Plant Physiol.* **142,** 1364–1379
44. Hofmann, B., Budde, H., Bruns, K., Guerrero, S. A., Kalisz, H. M., Menge, U., Montemartini, M., Nogoceke, E., Steinert, P., Wissing, J. B., Flohé, L., and Hecht, H. J. (2001) *Biol. Chem.* **382,** 459–471
45. Hirotsu, S., Abe, Y., Okada, K., Nagahara, N., Hori, H., Nishino, T., and Hakoshima, T. (1999) *Proc. Natl. Acad. Sci. U. S. A.* **96,** 12333–12338
46. Evrard, C., Capron, A., Marchand, C., Clippe, A., Wattiez, R., Soumillion, P., Knoops, B., and Declercq, J. P. (2004) *J. Mol. Biol.* **337,** 1079–1090
47. Karplus, P. A., and Hall, A. (2007) *Subcell. Biochem.* **44,** 41–60
48. Melchers, J., Dirdjaja, N., Ruppert, T., and Krauth-Siegel, R. L. (2007) *J. Biol. Chem.* **282,** 8678–8694
49. Burley, S. K., and Bonanno, J. B. (2002) *Curr. Opin. Struct. Biol.* **12,** 383–391
50. Alexander, P. A., He, Y., Chen, Y., Orban, J., and Bryan, P. N. (2007) *Proc. Natl. Acad. Sci. U. S. A.* **104,** 11963–11968
51. Platt, A., Ross, H. C., Hankin, S., and Reece, R. J. (2000) *Proc. Natl. Acad. Sci. U. S. A.* **97,** 3154–3159
52. Eisenmesser, E. Z., Bosco, D. A., Akke, M., and Kern, D. (2002) *Science* **295,** 1520–1523
53. Foloppe, N., and Nilsson, L. (2007) *J. Mol. Biol.* **372,** 798–816
54. Yang, Y. F., and Wells, W. W. (1991) *J. Biol. Chem.* **266,** 12759–12765
55. Wood, Z. A., Schröder, E., Robin Harris, J., and Poole, L. B. (2003) *Trends Biochem. Sci.* **28,** 32–40
56. Delaunay, A., Pflieger, D., Barrault, M. B., Vinh, J., and Toledano, M. B. (2002) *Cell* **111,** 471–481
57. Thompson, J. D., Gibson,T. J., Plewniak, F., Jeanmougin, F., and Higgins, D. G. (1997) *Nucleic Acids Res.* **24,** 4876–4882